Supplement of Atmos. Chem. Phys., 16, 4817–4835, 2016
http://www.atmos-chem-phys.net/16/4817/2016/
doi:10.5194/acp-16-4817-2016-supplement

Atmospheric Chemistry and Physics Open Access EGU

Supplement of

Modeling and measurements of urban aerosol processes on the neighborhood scale in Rotterdam, Oslo and Helsinki

Matthias Karl et al.

Correspondence to: Matthias Karl (matthias.karl@hzg.de)

S1. Approximation of the initial plume height at roadside

The initial stage of the exhaust plume was described with the simple plume dispersion model by Vignati et al. (1999). The approximation of the initial plume height, $H_{m,0}$, at roadside was done as an independent step prior to the scenario calculation. The expression by Vignati et al. (1999) for the evolution of the plume cross section was applied:

$$S(t) = \left(\sqrt{S_0} + t\,\sigma_w(0)\right)^2 - \left(t\,\alpha\,u_0\right)^2 \qquad \text{(S1)}$$

Where S is the cross sectional area of the plume or, in more statistically oriented way, it can be interpreted as being proportional to the variance of the Gaussian plume distribution. Further, S_0 is the size of the plume at the exhaust pipe (assumed to be equal to the cross-sectional area of the exhaust pipe, here using a radius of 0.020 m), $\sigma_w(0)$ is the initial entrainment velocity at $t = 0$ and u_0 is the initial exhaust gas velocity. The proportionality constant α is given a value of 0.1, which corresponds to typical levels of mechanically induced turbulence (Berkowicz et al., 1997). For $\sigma_w(0)$ a value of 0.25 m s^{-1} was adopted (Fig. 6 in Kastner-Klein et al., 2000), typical for traffic on working days between 8 a.m. and 7 p.m. in situations where traffic-induced turbulence dominates. For the initial exhaust gas velocity u_0 a value of 0.23 m s^{-1} typical for light-duty vehicles was taken (Kurkela et al., 1994). Further, t is the time from the release, here expressed as $t = x/U$. A fixed distance from the release point of x_{st} = 9 m was chosen for the PN measurement, resulting in an arrival time t_{st} at the measurement location which differs for different wind speeds. Solving the above expression for the initial plume height at roadside, assuming circular plume cross section, gives:

$$H_{m,0} = 2\sqrt{\frac{S(t_{st})}{\pi}} \qquad \text{(S2)}$$

For the wind speeds 1.0 m s^{-1}, 3.0 m s^{-1} and 4.0 m s^{-1} initial plume heights of 2.6 m, 0.9 m, and 0.7 m, respectively, were obtained at the roadside.

S2. Roadside concentrations of condensable organic vapors

In this study, particle growth was assumed to occur by condensation of gaseous n-alkanes which represent the typical range of volatility of vapors related to vehicle exhaust emissions. For the included roadside locations and campaigns, gas-phase concentration of n-alkanes and other condensable organic compounds have not been measured and therefore it is not known whether they were in equilibrium with the (bulk) particle phase or not. Such measurements are still rare and not complete regarding the full volatility spectrum of condensable organic vapors. Based on theoretical considerations, Zhang and Wexler (2004) concluded that during the second dilution stage, between roadside and a few hundred meters distant from the road, particles can still grow by condensation, although with decreasing growth rates when the air parcel moves away from the road.

Mandalakis et al. (2002) reported a total n-alkane (C14 – C33) concentration of 50.43 ng m^{-3} in the vapor phase and of 38.65 ng m^{-3} in the particulate phase, from measurements in the urban center of Athens (Greece). C14 – C23 n-alkanes were mainly in the vapor phase while C25 – C33 n-alkanes were mainly in the particulate phase; C24 was equally present in both phases. Summing up vapor concentrations for C14 – C23 and particulate phase concentrations for C25 – C33 and the phase averaged concentration for C24 gave a concentration of total condensable n-alkanes of 73.5 ng m^{-3}, corresponding to 5.1 ppt when using the averaged molecular weight of

C22 and C28. Similar total n-alkane concentrations were reported by Harrad et al. (2003) for an urban traffic site (Birmingham, UK), by Doskey and Andren (1986) for a rural site (North Wisconsin, WI, USA), and by Pietrogrande et al. (2011) for a suburban site (particulate phase only, Augsburg, Germany). Total n-alkane concentrations were several times higher at an urban industrial site (Prato, Italy) in a study by Cincinelli et al. (2007). Total n-alkane concentrations were more than one order of magnitude higher at an urban site in China (Bi et al., 2002). Although a concentration of 5 ppt of condensable n-alkanes seems to be typical for the urban environment, higher concentrations may occur. Other condensable organic compounds such as PAH, n-alkanols, and dicarboxylic acids are also emitted from vehicles and may contribute to the total concentration of condensable organic vapors at the roadside, which were represented by C22 and C28 in the aerosol dynamics model.

S3. Modification of the Brownian coagulation kernel to approximate van der Waals forces and viscous interactions

Van der Waals forces are weak dipole-dipole attractions in uncharged, nonpolar molecules caused by random fluctuations in the electron cloud. When a particle experiencing a brief charge fluctuation approaches another particle, the first induces a charge of the opposite sign on the nearest part of the other particle. Viscous forces are fluid mechanical interactions arising from the fact that velocity gradients induced by a particle approaching another particle in a viscous medium affect the motion of the other particle. Viscous forces retard the rate of van der Waals force enhancement in the continuum regime. It has been shown that van der Waals forces can enhance the coagulation rate of small particles by up to a factor of five (Jacobson and Seinfeld,

2004). However the degree of enhancement depends on the Hamaker constant A which is specific for the van der Waals properties of each substance. Jacobson and Seinfeld (2004) used a value of A/k_BT = 200 (k_B is the Boltzmann constant and T is the air temperature), which gave plausible enhancement for the coagulation of soot particles.

A simplified treatment of the van der Waals enhancement combined with retardation by viscous forces was considered sufficient to evaluate the possible uncertainty introduced into this study by neglecting the two interactions. A correction factor $V_{E,i,j}$ due to van der Waals and viscous forces was applied to the Brownian collision kernel in the MAFOR model:

$$K_{i,j}^{corr} = K_{i,j}^{B} \cdot V_{E,i,j} \tag{S3}$$

Based on Fig. 3 in Jacobson and Seinfeld (2004), three regimes of enhancement were distinguished in the implementation, depending on the value of the particle pair Knudsen number, Kn_p, of two colliding particles with radius r_i and r_j:

$$Kn_p = \frac{\sqrt{\lambda_{p,i}^2 + \lambda_{p,j}^2}}{r_i + r_j} \tag{S4}$$

Where λ_p is the effective mean free path of an individual particle. The three cases for the correction factor were approximated by:

$$V_{E,i,j} = \begin{cases} 1.0 & , Kn_p < 0.1 \\ 2.0 + 0.4 \cdot \ln\left(Kn_p\right) & , 0.1 \le Kn_p \le 10.0 \\ 3.0 & , Kn_p > 10.0 \end{cases} \tag{S5}$$

Clearly, $V_{Ei,j}$ for values of the particle pair Knudsen number greater than 1.0 depends on the radius ratio of the two colliding particles and can range from 1.0 to 5.0 for ratios between 50 and 1 when A/k_BT = 200 is used. A value (enhancement factor) of 3.0 was chosen which corresponds to a radius ratio of about 5, e.g. describing the collision of a 5 nm-particle with a 25 nm-particle, relevant for the studied size distributions at roadside. Figure S5 shows the predicted effect of van der Waals forces and viscous forces on Brownian coagulation for spherical as well as for fractal particles (using two different fractal geometries) when the volume-equivalent diameter of the first particle is 10 nm.

Table S1: Meteorological and dispersion conditions during the campaigns at the traffic sites. Notation: WD = wind direction, WS = wind speed, Ta = ambient air temperature, RH = relative humidity, L^{-1} = inverse Monin-Obukhov length (L^{-1}<0 unstable; L^{-1}=0 neutral, L^{-1}>0 stable), H_{mix} = mixing height. Rotterdam data and mixing height data: ranges of 10th and 90th percentile; median in brackets. Helsinki LIPIKA and MMEA: Ta and RH data as mean and standard deviation. All other data is given as range of minimum to maximum value. Atmospheric stability data for Helsinki was extracted from the CAR-FMI model. Stability data for Oslo and Rotterdam was calculated based on temperature and wind speed at two heights from nearby met stations using traditional Monin-Obukhov similarity theory.

City/ campaign	WD [°]	WS [m/s]	T_a [°C]	RH [%]	L^{-1} [m^{-1}]	H_{mix} [m]	Dispersion
Rotterdam	97−280 (226)	0.1−5 (3.6)	10.5−17.8 (14.8)	43−88 (71)	1e-3−1e-1	50−359 (128)	Varied
Oslo, UFP-Oslo Tav	66−238	0.8−6.3	-14−10	42−97	-4e-1−2e-1	16−983 (77)	Varied
Oslo, UFP-Oslo Winter	65−86	0.6−3.8	-12− -8	69−93	0	204−902 (549)	Varied
Helsinki, SAPPHIRE, Case1	-90−30	<4	10−15	60−95	-5e-3−1e-2	55−1386 (220)	Downwind
Helsinki, SAPPHIRE, Case2	-90−0	<5	-15− -4	55-92	5e-4−1e-2	132−408 (205)	Downwind
Helsinki, LIPIKA, Case1	250−300	1.3−2.8	1.9±0.5	80±1	4e-4−8e-3	92−179 (149)	Downwind
Helsinki, MMEA	10−50	4−5	-9.7±0.7	68±4	2e-3−8e-3	115−174 (144)	Downwind

Table S2: Results from sensitivity tests for dry deposition using two deposition methods, KS2012 and H2012. Sensitivity runs were done for the campaigns in Rotterdam and Oslo UFP-Oslo Tav under moderate dispersion conditions. The contribution of dry deposition to percentage change of PN concentration (%) between roadside station and neighborhood environment after 30 minutes transport time. The result for KS2012 in case "Urban" corresponds to the contribution of dry deposition to PN change in the reference model simulation.

Case	Surface type	Rotterdam (KS2012)	Rotterdam (H2012)	Oslo UFP-Oslo Tav (KS2012)	Oslo UFP-Oslo Tav (H2012)
Urban	Street and building	4.3	2.6	2.6	1.2
Low friction	Street and building	4.2	0.5	2.5	0.3
High roughness	Street and building	4.3	12.8	2.6	4.2
Green area without trees	Grassland	3.0	0.6	1.8	0.3
Green area with forest	Deciduous forest	2.0	13.9	1.2	4.5

Table S3: Data required for the implementation of the PNC parameterization for dry deposition and for coagulation using six PNC size categories. MAFOR uses a large number of bin sizes so the extracted coefficients for the six size categories are based on an integral/average over a number of bins in the model. The initial size distribution ratio is the PN fraction in each PNC category for the "mean of traffic sites" distribution.

Size category	Size ranges [nm]	Initial size distrib. ratio [−]	v_d KS2012 [cm s^{-1}]	K_{coag} [cm^3 s^{-1}]
PNC_1	8.5−25	0.70	0.53	4.51e-9
PNC_2	25−50	0.15	0.18	1.50e-8
PNC_3	50−75	0.07	0.068	5.40e-9
PNC_4	75−100	0.07	0.039	6.26e-9
PNC_5	100−200	0.003	0.023	2.28e-9
PNC_6	200−500	0.007	0.024	8.69e-10

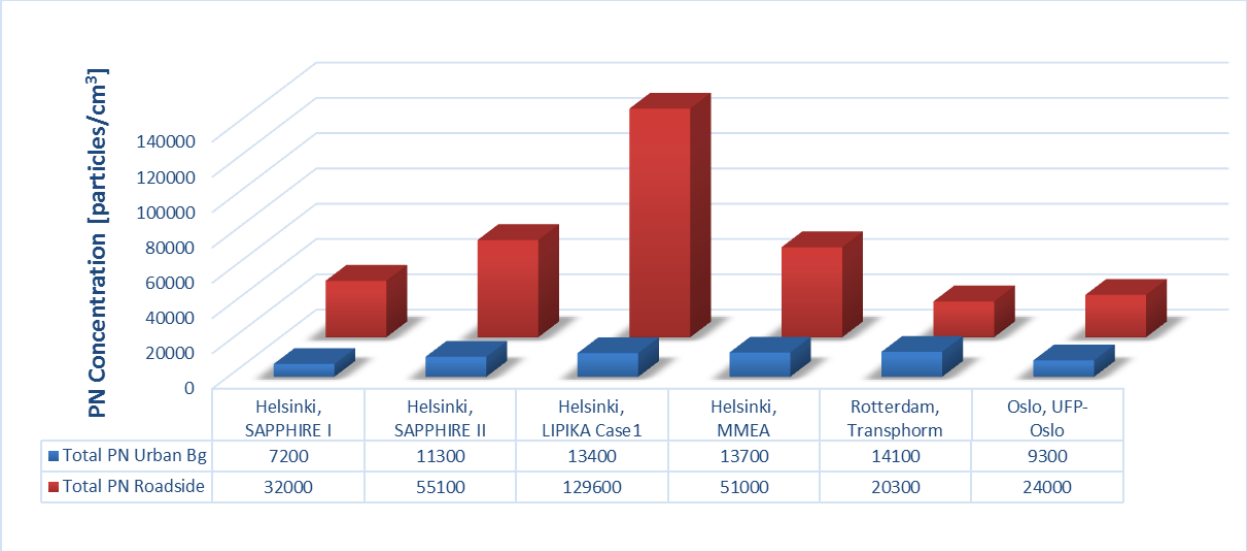

	Helsinki, SAPPHIRE I	Helsinki, SAPPHIRE II	Helsinki, LIPIKA Case1	Helsinki, MMEA	Rotterdam, Transphorm	Oslo, UFP-Oslo
Total PN Urban Bg	7200	11300	13400	13700	14100	9300
Total PN Roadside	32000	55100	129600	51000	20300	24000

Figure S1: Total PN concentration (in particles cm^{-3}) as measured campaign average at the roadside traffic station (red bars) and at the urban background site (blue bars) for all campaigns included in this study.

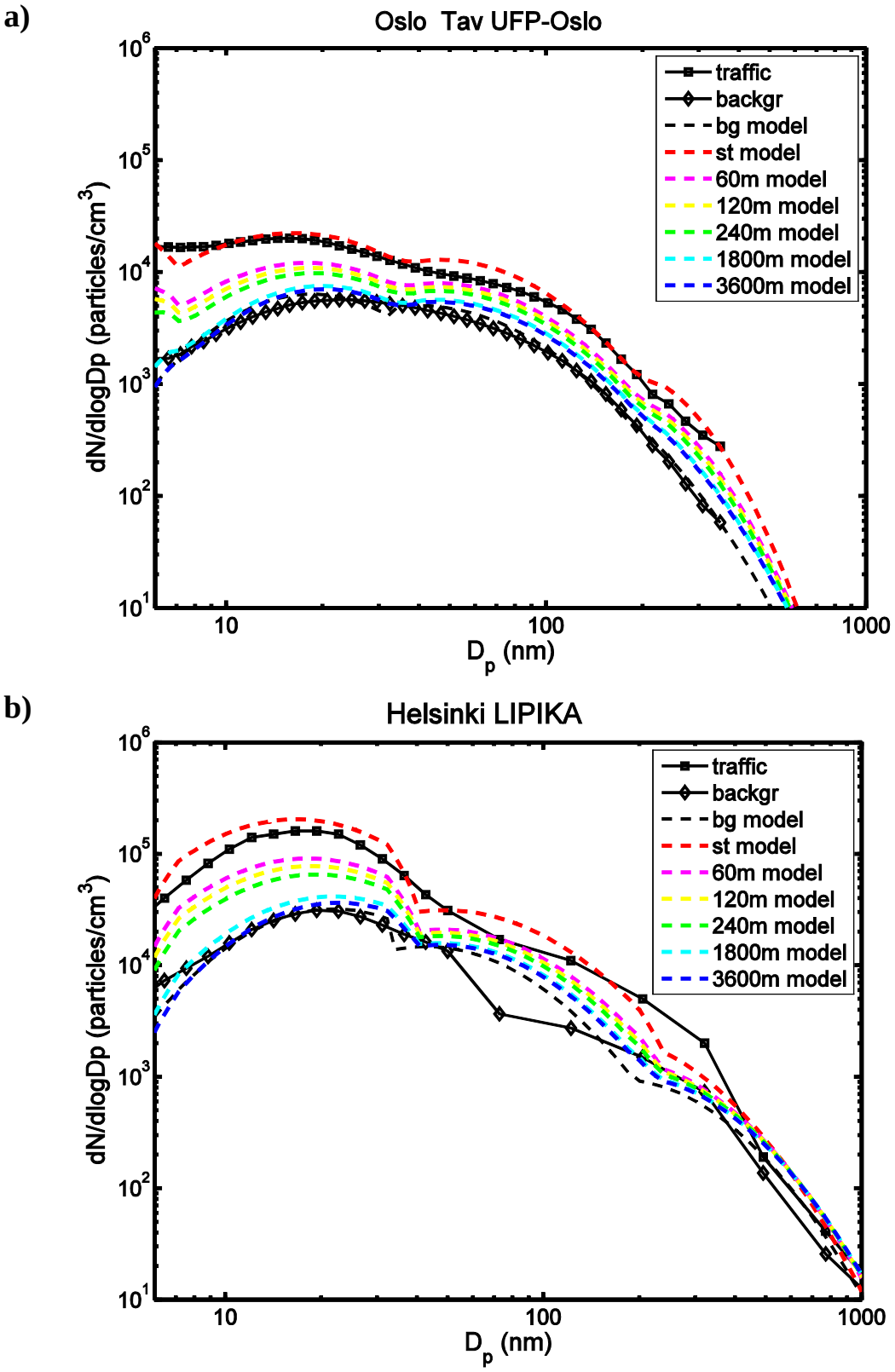

Figure S2: Continued.

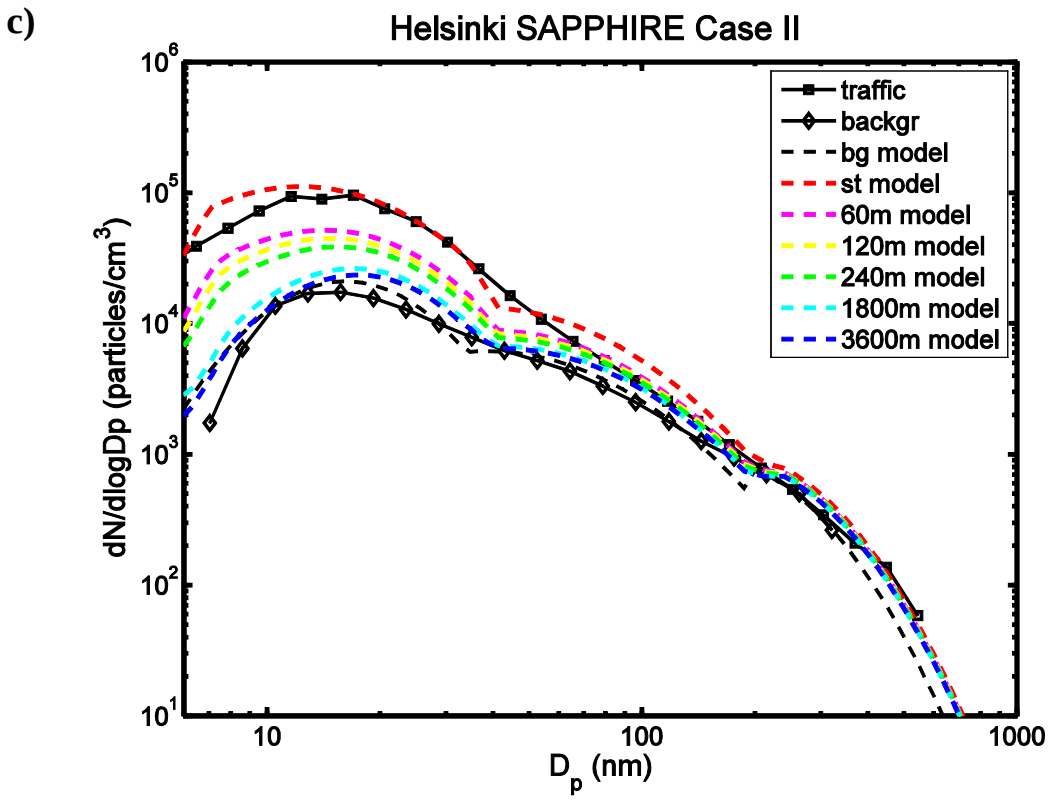

Figure S2: Size distributions (dN/dlogDp in particles cm^{-3}) downwind of roads in selected campaigns: a) Oslo UFP-Oslo Tav, b) Helsinki LIPIKA, and c) Helsinki SAPPHIRE Case II. The plots show the measured distribution at roadside (black squares connected by line), the measured distribution at urban background (black diamonds connected by line), the initial model distribution (roadside: dashed red line, background: dashed black line) and the modeled distributions (resulting for moderate dispersion conditions) at distances of 60, 120, 240, 1800, and 3600 m, respectively. Size distributions are shown with a lower size cut-off at 6 nm.

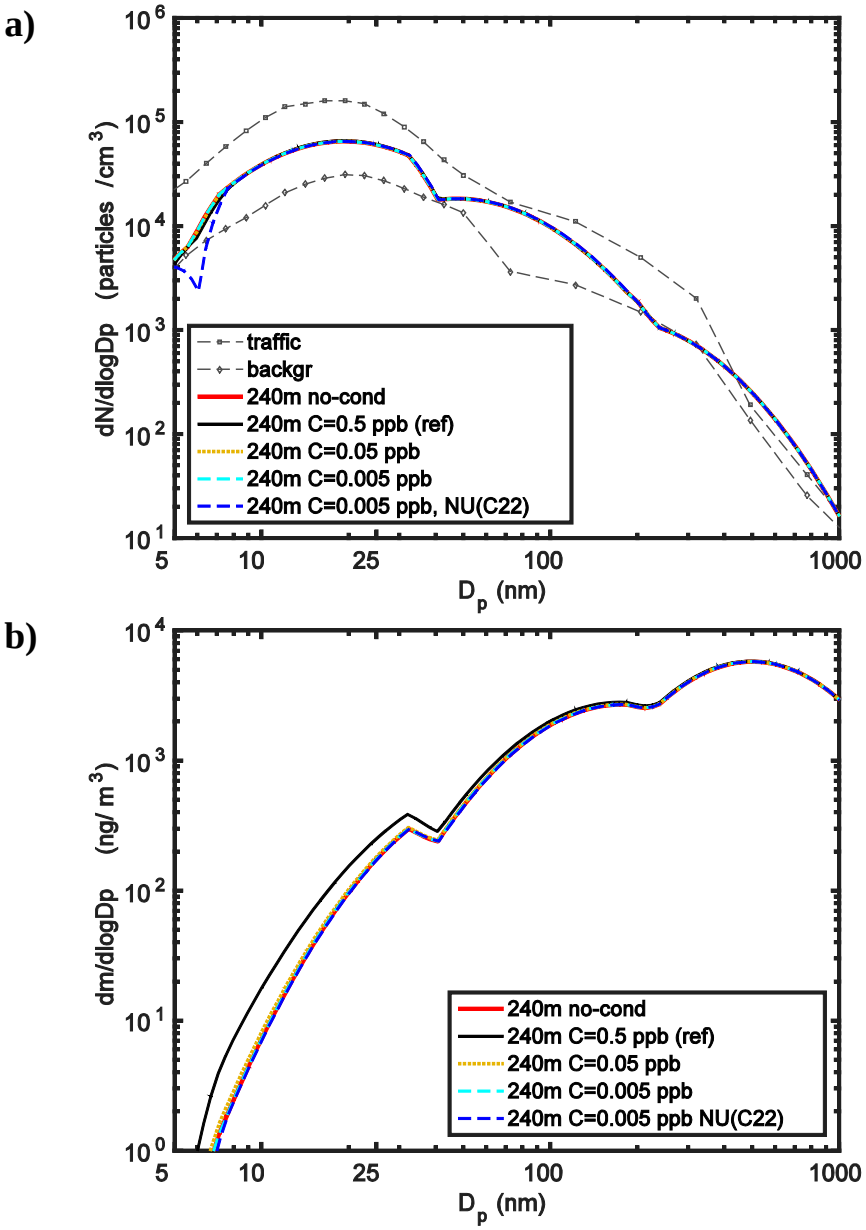

Figure S3: Sensitivity of the modeled size distribution to changes of the concentration of condensable organic vapors (sum of C22 and C28) and composition of particles in campaign Helsinki LIPIKA for moderate dispersion: a) number size distributions ($dN/dlogD_p$ in particles cm^{-3}), and b) mass size distribution ($dm/dlogD_p$ in ng m^{-3}). Size distributions 240 m downwind for reference case with 0.5 ppb (black line), case 0.05 ppb (yellow dots), case 0.005 ppb (cyan dashes), and case 0.005 ppb with 100% C22 for D_p < 10 nm particles (blue dashes) are compared to case without condensation and evaporation (red line).

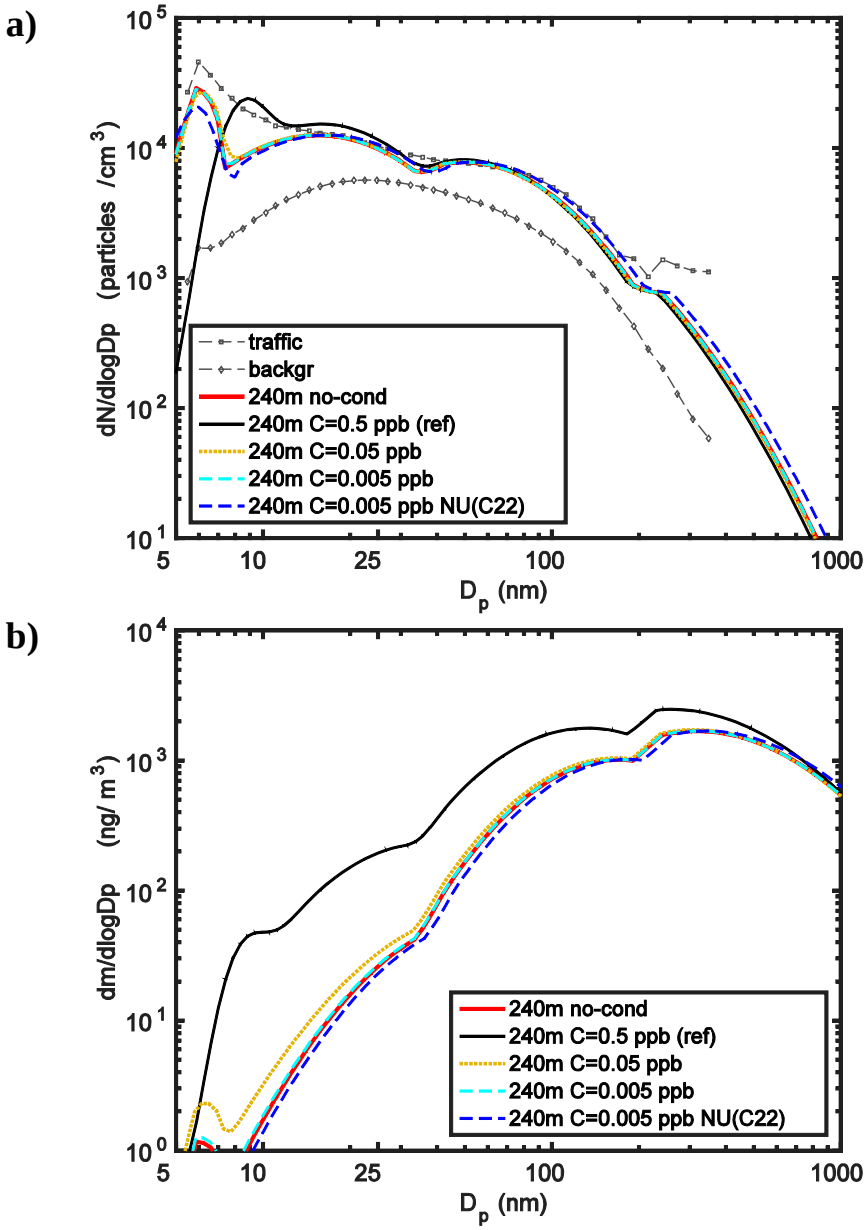

Figure S4: Sensitivity of the modeled size distribution to changes of the concentration of condensable organic vapors (sum of C22 and C28) and composition of particles in campaign Oslo UFP-Oslo Winter for inefficient dispersion: a) number size distributions ($dN/dlogD_p$ in particles cm^{-3}), and b) mass size distribution ($dm/dlogD_p$ in ng m^{-3}). Size distributions 240 m downwind for reference case with 0.5 ppb (black line), case 0.05 ppb (yellow dots), case 0.005 ppb (cyan dashes), and case 0.005 ppb with 100% C22 for $D_p < 10$ nm particles (blue dashes) are compared to case without condensation and evaporation (red line).

a)

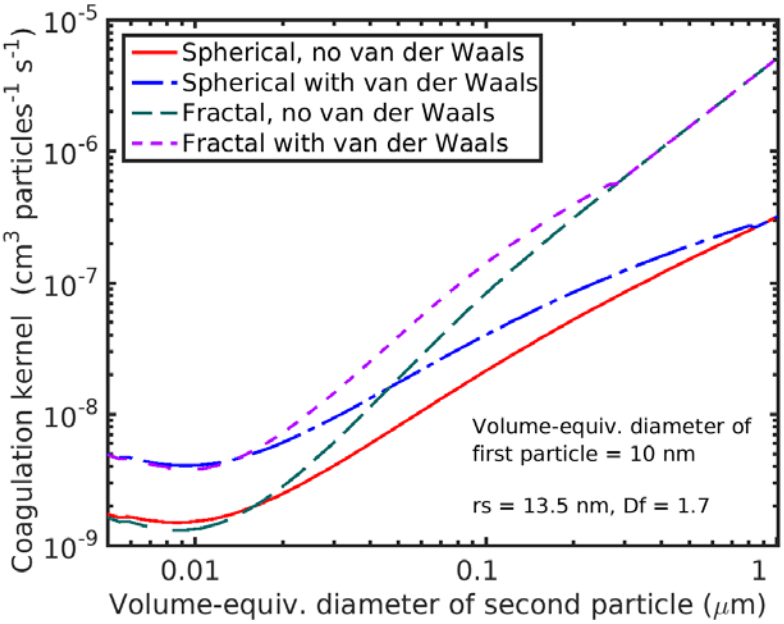

b)

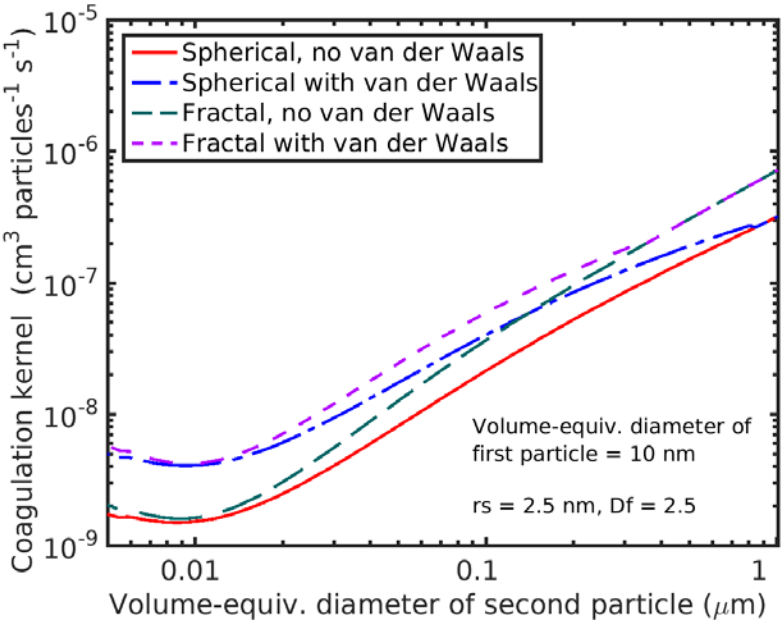

Figure S5: Brownian coagulation when the volume-equivalent diameter of the first particle is 10 nm and the volume-equivalent diameter of the second particle varies from 5 to 1000 nm: a) fractal geometry (r_s = 13.5 nm, D_f = 1.7) adapted from Jacobson and Seinfeld (2004), b) fractal geometry (r_s = 2.5 nm, D_f = 2.5) adapted from Lemmetty et al. (2008). The four curves account for when particles are spherical or fractal and when van der Waals and viscous forces (parameterized as described in section S3) are or are not included.

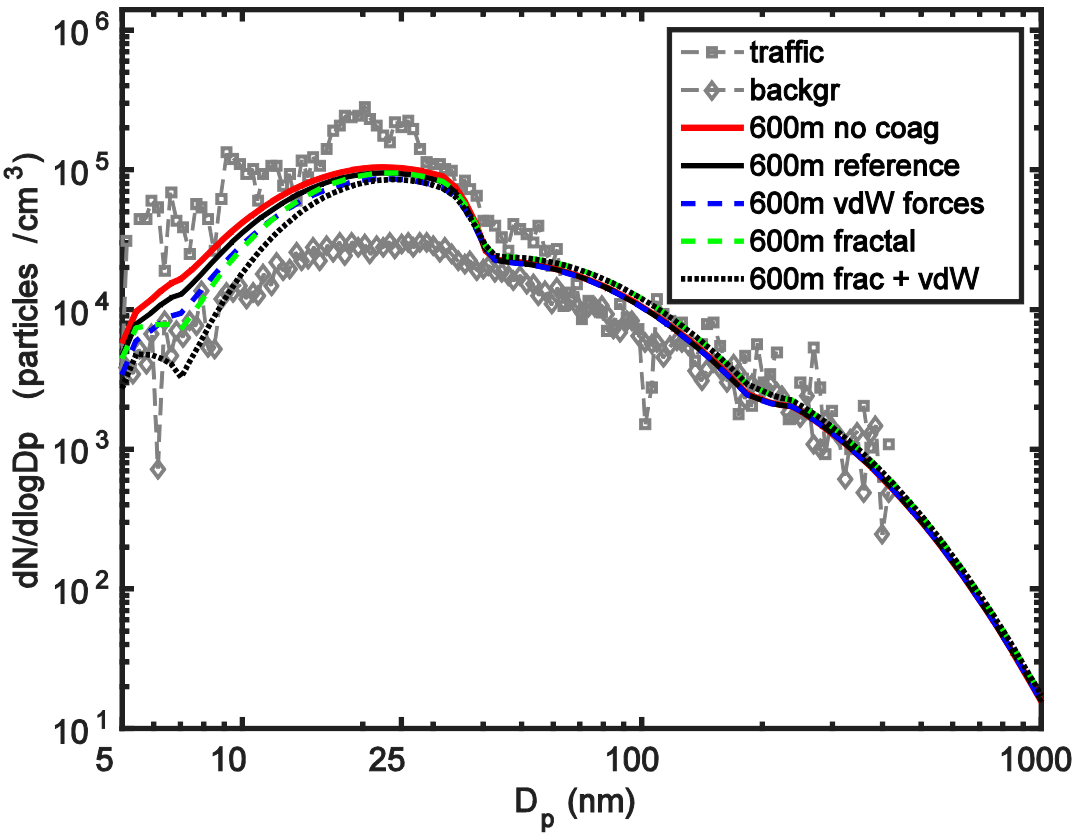

Figure S6: Sensitivity of the modeled size distribution to the effects of fractal geometry and van der Waals forces combined with viscous forces in campaign Helsinki-MMEA for inefficient dispersion. Modeled number size distributions ($dN/dlogD_p$ in particles cm^{-3}) 600 m downwind for reference case, i.e. spherical particles, coagulation by Brownian motion only (black line), case with coagulation of spherical particles enhanced by van der Waals and viscous forces (blue dashes), case with fractal geometry (green dashes) according to Jacobson and Seinfeld (2004), and case with coagulation of fractal particles enhanced by van der Waals and viscous forces (black dots). Red curve shows the modeled size distribution for the case without coagulation.

References

Bi, X., Sheng, G., Peng, P., Chen, Y., Zhang, Z., and Fu, J.: Distribution of particulate- and vapor-phase n-alkanes and polycyclic aromatic hydrocarbons in urban atmosphere of Guangzhou, China, Atmos. Environ., 37, 289-298, 2002.

Berkowicz, R., Hertel, O., Sørensen, N. N., and Michelsen J. A.: Modelling air pollution from traffic in urban areas. In: Perkins, R. J., Belcher, S. E., editors, Flow and dispersion through groups of obstacles, Oxford: Clarendon Press, 121-141, 1997.

Cincinelli, A., Del Bubba, M., Martellini, T., Gambaro, A., and Lepri, L.: Gas-particle concentration and distribution of n-alkanes and polycyclic aromatic hydrocarbons in the atmosphere of Prato (Italy), Chemosphere, 68, 472-478, 2007.

Doskey, P. V. and Andren A. W.: Particulate- and vapor-phase n-alkanes in the northern Wisconsin atmosphere, Atmos. Environ., 20(9), 1735-1744, 1986.

Harrad, S., Hassoun, S., Callen Romero, M.S., and Harrison, R. M.: Characterisation and source attribution of the semi-volatile organic content of atmospheric particles and associate vapour phase in Birmingham, UK, Atmos. Environ., 37, 4985-4991, 2003.

Jacobson, M. Z. and Seinfeld, J. H.: Evolution of nanoparticle size and mixing state near the point of emission, Atmos. Environ., 38, 1839-1850, 2004.

Kastner-Klein, P., Berkowicz, R., and Plate, E. J.: Modelling of vehicle induced turbulence in air pollution studies for streets, Int. Journal of Environment and Pollution, 14(1-6), 496-507, doi: 10.1504/IJEP.2000.000573, 2000.

Kurkela, J., Valmari, T., and Kauppinen, E.: The 14.9.-15.9.1994 particulate phase measurements of a bus diesel engine, VTT Aerosol Research Group Publications, Espoo, 18pp. (in Finnish), 1994.

Lemmetty, M., Rönkkö, T., Virtanen, A., Keskinen, J., and Pirjola, L.: The effect of Sulphur in diesel exhaust aerosol: Models compared with measurements, Aerosol Sci. Technol., 42, 916-929, 2008.

Mandalakis, M., Tsapakis, M., Tsoga, A., and Stephanou, E. G.: Gas-particle concentrations and distribution of aliphatic hydrocarbons, PAHs, PCBs and PCDD/Fs in the atmosphere of Athens (Greece), Atmos. Environ., 36, 4023-4035, 2002.

Pietrogrande, M. C., Abbaszade,, G., Schnelle-Kreis, J., Bacco, D., Mercuriali, M., and Zimmermann, R.: Seasonal variation and source estimation of organic compounds in urban aerosol of Augsburg, Germany, Environmental Pollution, 159, 1861-1868, 2011.

Vignati, E., Berkowicz, R., Palmgren, F., Lyck, E., and Hummelshøj, P.: Transformations of size distributions of emitted particles in streets, Science of the Total Environment, 235, 37-49, 1999.

Zhang, K .M. and Wexler, A. S.: Evolution of particle number distribution near roadways – Part I: Analysis of aerosol dynamics and its implications for engine emission measurement, Atmos. Environ., 38, 6643–6653, 2004.